Analytic model for the single-mode Richtmyer-Meshkov instability: from the linear to the nonlinear regime

Marc Vandenboomgaerde[1] and Olivier Lafitte[2,3]

1- Commissariat à l'Energie Atomique, DAM/Ile de France BP12, 91680 Bruyères-Le-Châtel, France
2- LAGA-Institut Galilée, Université Paris XIII, France
3- Commissariat à l'Energie Atomique, Saclay, DM2S, France
marc.vandenboomgaerde@cea.fr and olivier.lafitte@cea.fr

1. Introduction

The Richtmyer-Meshkov instability (IRM) is involved in several physical phenomena such as, for example, inertial confinement fusion (ICF) or supernovas. This instability occurs at the interface between two materials at the passage of a shock wave. Any perturbation of this interface first grows linearly, then nonlinearly; at late time, complex structures appear at the interface which then reaches a pre-turbulent regime. These perturbations can break the symmetry of the implosion in an ICF capsule and decrease its fusion yield.
The nonlinear regime of the IRM, in the planar geometry, has been studied by numerous authors who derived algebraic solutions[1,2,3] . They have a limited range of validity due to a secular behaviour which leads to a divergence of the series in time. As a result, only the weakly nonlinear stage of the IRM can be studied by these methods.

This paper is an attempt to solve this problem by describing the nonlinear growth of the IRM with ordinary differential equations. First, the equations which describe the dynamics of a planar single-mode interface are simplified by using a change of variable. Then, some hypotheses are made in order to find a non-divergent solution.

The paper is organized as follows. In Sec. 2, we detail the derivation of a new nonlinear theory. In Sec. 3, some comparisons between this model, experiments, simulations and others theories are presented. In Sec. 4, we discuss the results and the range of validity of our model.

2. Theoretical derivation

We consider a single-mode sinusoidal perturbation, described by $z=\eta(x,t)$ between two gases (see Fig.1). The fluids are considered inviscid and incompressible. The flow is supposed irrotational and the velocity in each fluid derives from a potential. The Atwood number is defined as $At=(\rho'-\rho)/(\rho'+\rho)$. The equations that have to be solved are the Laplacian equation for the potentials, the motion equation of the interface in each fluid (Eq.1), and the Bernoulli's equation at the interface (Eq.2).

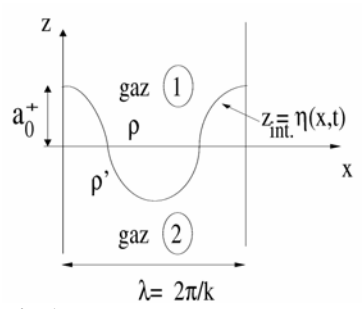

Fig.1 *: Sketch of the configuration*

$$\begin{cases} \dfrac{\partial\Phi}{\partial z}=\dfrac{\partial\eta}{\partial t}-\dfrac{\partial\Phi}{\partial x}\dfrac{\partial\eta}{\partial x} \\ \qquad\qquad\qquad\qquad \text{at } z=\eta \\ \dfrac{\partial\Phi'}{\partial z}=\dfrac{\partial\eta}{\partial t}-\dfrac{\partial\Phi'}{\partial x}\dfrac{\partial\eta}{\partial x} \end{cases} \tag{1}$$

$$-\rho'\frac{\partial\Phi'}{\partial t}+\rho\frac{\partial\Phi}{\partial t}+\frac{1}{2}\rho'[(\frac{\partial\Phi'}{\partial x})^2+(\frac{\partial\Phi'}{\partial z})^2]-\frac{1}{2}\rho[(\frac{\partial\Phi}{\partial x})^2+(\frac{\partial\Phi}{\partial z})^2]=0 \text{ at } z=\eta \tag{2}$$

In order to simplify these equations, we use the following change of variable (Eq.3) :

$$\begin{cases} X=x \\ Z=z-\eta(x,t) \\ T=t \end{cases} \tag{3}$$

This leads to a new set of equations (Eqs. 4-5), for the Laplacian, motion and Bernoulli's equations, respectively:

$$\begin{cases} \dfrac{\partial^2\Phi}{\partial X^2}+\dfrac{\partial^2\Phi}{\partial Z^2}\left(1+(\dfrac{\partial\eta}{\partial X})^2\right)=\dfrac{\partial^2\eta}{\partial X^2}\dfrac{\partial\Phi}{\partial Z}+2\dfrac{\partial\eta}{\partial X}\dfrac{\partial^2\Phi}{\partial X\partial Z} \\ \dfrac{\partial^2\Phi'}{\partial X^2}+\dfrac{\partial^2\Phi'}{\partial Z^2}\left(1+(\dfrac{\partial\eta}{\partial X})^2\right)=\dfrac{\partial^2\eta}{\partial X^2}\dfrac{\partial\Phi'}{\partial Z}+2\dfrac{\partial\eta}{\partial X}\dfrac{\partial^2\Phi'}{\partial X\partial Z} \end{cases} \quad \text{at } Z=0 \qquad \textbf{(4)}$$

$$\begin{cases} \dfrac{\partial\eta}{\partial T}\quad\left(\dfrac{\partial\Phi}{\partial X}\quad\dfrac{\partial\eta}{\partial X}\dfrac{\partial\Phi}{\partial Z}\right)\dfrac{\partial\eta}{\partial X}+\dfrac{\partial\Phi}{\partial Z}=0 \\ \dfrac{\partial\eta}{\partial T}\quad\left(\dfrac{\partial\Phi'}{\partial X}\quad\dfrac{\partial\eta}{\partial X}\dfrac{\partial\Phi'}{\partial Z}\right)\dfrac{\partial\eta}{\partial X}+\dfrac{\partial\Phi'}{\partial Z}=0 \end{cases} \quad \text{at } Z=0 \qquad \textbf{(5)}$$

$$\begin{array}{l} \rho'\dfrac{\partial\Phi'}{\partial T}+\dfrac{1}{2}\left[(\dfrac{\partial\Phi'}{\partial X})^2\quad(\dfrac{\partial\Phi'}{\partial Z})^2(1+(\dfrac{\partial\eta}{\partial X})^2))\right]= \\ \rho\dfrac{\partial\Phi}{\partial T}+\dfrac{1}{2}\left[(\dfrac{\partial\Phi}{\partial X})^2\quad(\dfrac{\partial\Phi}{\partial Z})^2(1+(\dfrac{\partial\eta}{\partial X})^2))\right]\quad\text{at } Z=0 \end{array} \qquad \textbf{(6)}$$

In a previous model[1], which used perturbations methods, the interface and the velocity potentials could be written as:

$$\begin{cases} \eta(x,t)=\sum_{n=1}^{+\infty}\eta^{(n)}(x,t) & k\eta^{(n)}=(a_0k\sigma t)^n\sum_{j=1}^{n}a_j^n cos(jkx) \\ \Phi(x,z,t)=\sum_{n=0}^{+\infty}\Phi^{(n)}(x,z,t) \quad \text{with} & \dfrac{k^2}{\sigma}\Phi^{(n)}=(a_0k)^n(\sigma t)^{n-1}\sum_{j=0}^{n}b_j^n\,cos(jkx)\,e^{-jkz} \\ \Phi'(x,z,t)=\sum_{n=0}^{+\infty}\Phi'^{(n)}(x,z,t) & \dfrac{k^2}{\sigma}\Phi'^{(n)}=(a_0k)^n(\sigma t)^{n-1}\sum_{j=0}^{n}b'^n_j\,cos(jkx)\,e^{jkz} \end{cases} \qquad \textbf{(7)}$$

In these equations, a_0, k, $a_0\sigma$, are the post-shocked amplitude of the perturbation, its wave number, and the initial growth rate of the instability, respectively. A non-dimensional time can be defined by $\tau=a_0\,k\sigma t$. Perturbation methods lead to divergent results for $\tau\approx1$, as shown on Fig. 2.

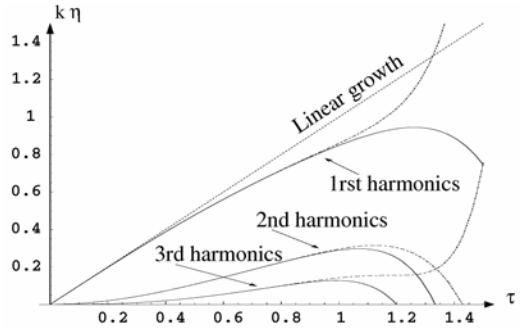

Fig. 2*: Growth of the first three modes obtained with perturbation methods. Full and dashed line are from 11th and 13th order results, respectively.*

In order to build a new approach, we use the following expression for the interface: $\eta(x,t)=\sum_{i=1}^{\infty}A_i(t)\cos kx$, where the $A_i(t)$ are supposed to be continuous monotonic functions of time. For the classical perturbation method, the main hypothesis was: $A_1 >> A_2 >> A_3 >> ...$ With the new model, this hypothesis evolves with τ: as τ grows, the $A_i(t)$ are no more negligible and become of the same order. Let us remark that the perturbation method is exact for $\tau<1$; so, classical and new approaches must match asymptotically for $\tau=1$.

In order to solve Eqs. 4-6, several hypotheses are made:
- the potential velocities are written as in Eqs. 8
- the dynamics of the interface is controlled by the $B_{i,i}$ (see Eqs. 8). This leads to Eqs.9 for the motion equation, and to a set of ordinary differential of equations for the $B_{i,i}$ for the Bernoulli's equation
- the $B_{i,j}$ are computed in order to cancel the divergent terms which are created by the $B_{i,i}$

$$\Phi(X,Z,T)=\sum_{i=0}^{+\infty}\phi_i(Z,T)\ \ cos(ikX) \qquad \text{with}$$

$$\begin{cases} \phi_0(Z,T)=B_{0,0}(T)+B_{0,1}(T)e^{-\frac{kZ}{\sqrt{(1)}}}+B_{0,2}(T)e^{-\frac{2kZ}{\sqrt{(2)}}}+B_{0,3}(T)e^{-\frac{3kZ}{\sqrt{(3)}}}+... \\ \phi_1(Z,T)=\quad B_{1,1}(T)e^{-\frac{kZ}{\sqrt{(1)}}}+B_{1,2}(T)e^{-\frac{2kZ}{\sqrt{(2)}}}+B_{1,3}(T)e^{-\frac{3kZ}{\sqrt{(3)}}}+... \\ \phi_2(Z,T)=\quad B_{2,2}(T)e^{-\frac{2kZ}{\sqrt{(2)}}}+B_{2,3}(T)e^{-\frac{3kZ}{\sqrt{(3)}}}+... \\ \phi_3(Z,T)=\quad B_{3,3}(T)e^{-\frac{3kZ}{\sqrt{(3)}}}+... \\ ... \end{cases} \tag{8}$$

$$\dot{A_i}=\frac{ikB_{i,i}}{\sqrt{(i)}} \quad \text{and} \quad B_{i,i}=-B'_{i,i} \tag{9}$$

As divergent terms, or terms leading to unphysical behaviour of the solutions are cancelled out by the $B_{i,j}$, the following systems are obtained (Eqs. 10-12):

- with one mode :

$$\begin{cases} \dot{A_1}(T)=\dfrac{kB_{1,1}(T)}{\sqrt{1+\frac{1}{4}k^2A_1^2(T)}} \\ \dot{B_{1,1}}(T)=0 \end{cases} \tag{10}$$

- with two modes :

$$\begin{cases} \dot{A_1}=\dfrac{kB_{1,1}}{\sqrt{1+\frac{1}{4}k^2A_1^2+2k^2A_2^2}} \\ \dot{A_2}=\dfrac{2kB_{2,2}}{\sqrt{1+\frac{1}{2}k^2A_1^2+A_2^2}} \\ \dot{B_{1,1}}=At\left(k^2A_1A_2\dfrac{k^2B_{2,2}^2}{1+\frac{1}{2}k^2A_1^2+k^2A_2^2}+k^2B_{1,1}B_{2,2}(\dfrac{1+k^2A_2^2}{\sqrt{1+\frac{1}{4}k^2A_1^2+2k^2A_2^2}\sqrt{1+\frac{1}{2}k^2A_1^2+A_2^2}}-1)\right) \\ \dot{B_{2,2}}=At\left(\dfrac{1}{4}\dfrac{k^2B_{1,1}^2(1+k^2A_2^2)}{1+\frac{1}{4}k^2A_1^2+2k^2A_2^2}-\dfrac{3}{4}k^2A_1^2\dfrac{k^2B_{2,2}^2}{1+\frac{1}{2}k^2A_1^2+A_2^2}\right) \end{cases} \tag{11}$$

- with three modes :

$$\begin{cases} \dot{A_1}=\dfrac{kB_{1,1}}{\sqrt{1+\frac{1}{4}k^2A_1^2+2k^2A_2^2+\frac{9}{2}k^2A_3^2}} \\ \dot{A_2}=\dfrac{2kB_{2,2}}{\sqrt{1+\frac{1}{2}k^2A_1^2+A_2^2+\frac{9}{2}k^2A_3^2}} \\ \dot{A_3}=\dfrac{3kB_{3,3}}{\sqrt{1+\frac{1}{2}k^2A_1^2+2A_2^2+\frac{9}{4}k^2A_3^2}} \\ \dot{B_{1,1}}=At\left(-k^2B_{1,1}B_{2,2}(1-\dfrac{1+k^2A_2^2+\frac{3}{2}k^2A_1A_3+\frac{5}{2}k^2A_3^2}{\sqrt{1+\frac{1}{4}k^2A_1^2+2k^2A_2^2+\frac{9}{2}k^2A_3^2}\sqrt{1+\frac{1}{2}k^2A_1^2+A_2^2+\frac{5}{2}k^2A_3^2}})\right. \\ -3k^2B_{2,2}B_{3,3}+kA_2\dfrac{k^2B_{2,2}^2}{1+\frac{1}{2}k^2A_1^2+A_2^2+\frac{9}{2}k^2A_3^2}(kA_1+3kA_3) \\ \left.-\dfrac{1}{2}k^2A_1A_2\dfrac{3k^2B_{1,1}B_{3,3}}{\sqrt{1+\frac{1}{4}k^2A_1^2+2k^2A_2^2+\frac{3}{2}A_1A_3+\frac{9}{2}k^2A_3^2}\sqrt{1+\frac{1}{2}k^2A_1^2+2A_2^2+\frac{9}{4}k^2A_3^2}}\right) \\ \dot{B_{2,2}}=At\left(\dfrac{1}{4}\dfrac{k^2B_{1,1}^2}{1+\frac{1}{4}k^2A_1^2+2k^2A_2^2+\frac{9}{2}k^2A_3^2}(1+k^2A_2^2+\dfrac{3}{2}k^2A_1A_3+\dfrac{9}{2}k^2A_3^2)\right. \\ +k^2A_1A_2\dfrac{k^2B_{1,1}B_{2,2}}{\sqrt{1+\frac{1}{2}k^2A_1^2+A_2^2+\frac{9}{2}k^2A_3^2}\sqrt{1+\frac{1}{2}k^2A_1^2+2A_2^2+\frac{5}{2}k^2A_3^2}}-\dfrac{3}{2}k^2B_{2,2}B_{3,3} \\ \left.-\dfrac{3}{4}k^2A_1^2\dfrac{k^2B_{2,2}^2}{1+\frac{1}{2}k^2A_1^2+A_2^2+\frac{9}{2}k^2A_3^2}-3k^2A_1A_2\dfrac{k^2B_{2,2}B_{3,3}}{\sqrt{1+\frac{1}{2}k^2A_1^2+A_2^2+\frac{9}{2}k^2A_3^2}\sqrt{1+\frac{1}{2}k^2A_1^2+2A_2^2+\frac{9}{4}k^2A_3^2}}\right) \\ \dot{B_{3,3}}=At\left(-\dfrac{1}{4}k^2A_1A_2(\dfrac{k^2B_{1,1}^2}{1+\frac{1}{4}k^2A_1^2+2k^2A_2^2+\frac{9}{2}k^2A_3^2}+\dfrac{4k^2B_{2,2}^2}{1+\frac{1}{2}k^2A_1^2+A_2^2+\frac{5}{2}k^2A_3^2}+\dfrac{27k^2B_{3,3}^2}{1+\frac{1}{2}k^2A_1^2+2A_2^2+\frac{9}{4}k^2A_3^2})\right. \\ +\dfrac{k^2B_{1,1}B_{2,2}}{\sqrt{1+\frac{1}{4}k^2A_1^2+2k^2A_2^2+\frac{9}{2}k^2A_3^2}\sqrt{1+\frac{1}{2}k^2A_1^2+A_2^2+\frac{5}{2}k^2A_3^2}}(1+\dfrac{1}{4}k^2A_1^2+k^2A_2^2+\dfrac{9}{4}k^2A_3^2) \\ \left.-\dfrac{6k^2B_{2,2}B_{3,3}}{\sqrt{1+\frac{1}{2}k^2A_1^2+A_2^2+\frac{9}{2}k^2A_3^2}\sqrt{1+\frac{1}{2}k^2A_1^2+2A_2^2+\frac{5}{4}k^2A_3^2}}(\dfrac{1}{4}k^2A_1^2+\dfrac{1}{2}k^2A_2^2-\dfrac{3}{4}k^2A_1A_3)\right) \end{cases} \tag{12}$$

These equations lead to saturated growths of each harmonics, as shown on Figs.3-5 for *At=1*.

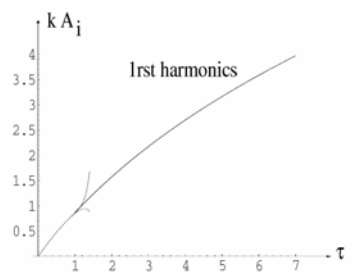

Fig. 3: *Growth of harmonics from Eq.10. Asymptotic matching with perturbation theory is done for* $\tau \approx 1$. *At=1.*

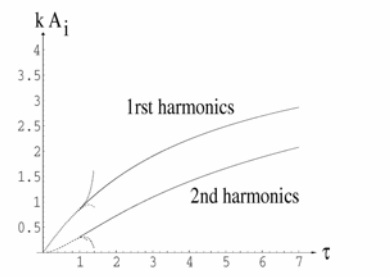

Fig. 4: *The same as in Fig.3, but for Eq.11.*

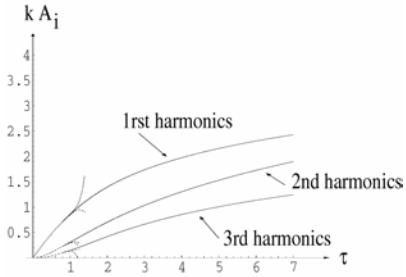

Fig. 5: *The same as in Fig.3, but for Eq.12.*

The solutions of Eqs. 10-12 are obtained numerically with symbolic computation software. However, such results are not exact solutions of Eqs. 4-6: once put back in this system, some small residues remain. So, Eq. 12 gives only a "pseudo-solution" that we believe is a good approximation of the exact solution. In order to prove this assumption, a linearization near this pseudo-solution must be derived, and the correction must be proven small. Such a mathematical proof is in progress. On the other hand, comparisons with experiments or simulations can be done in order to study the validity of the pseudo-solution.

3. Validation of the model and quantitative results

Simulations of a shock tube experiment[4] have been carried out by the CEA hydro-code TRICLADE[5]. The post-shocked Atwood number is 0.635. Gases are a mix of air and acetone, and SF_6. The Mach number of the incident shock wave is 1.3. The initial perturbation is a single-mode sinusoidal. The growth of the first three harmonics is presented in Fig.6, for numerical and theoretical results. In this figure, initial conditions of the nonlinear model are computed by matching with small perturbation method[1]; furthermore, a compressible linear[6] growth rate has been used for small τ. In Fig. 7, the initial conditions of the model are obtained by fitting with the numerical results.

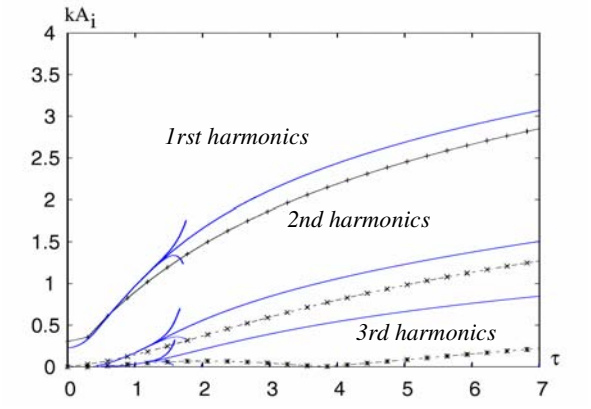

Fig. 6: *Growth of the first three harmonics for the shock tube experiment[4]. Curves with symbols and full ones are from simulation and model, respectively.*

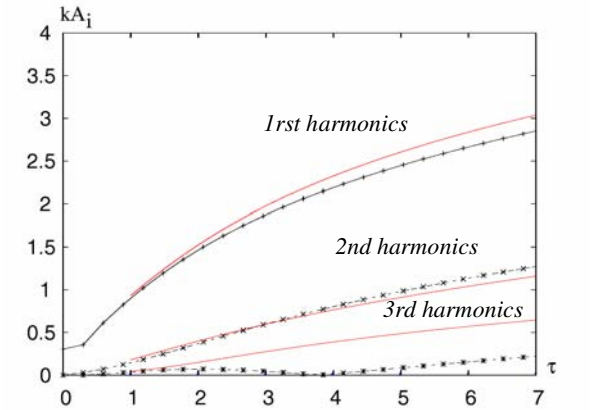

Fig. 7: *The same as in Fig. 6, but the initial conditions of the nonlinear model are obtained by fitting with simulation.*

For the first two harmonics, the agreement between simulation and theory is good; it is even better as the fitting with simulation is used. The model over-estimates the simulation for the third mode, but the latter has an odd behaviour in the simulation.

The physical parameters of this simulation were taken from a shock tube experiment[4]. Experimental data about the half peak-to-valley amplitude can be compared with the nonlinear model (see Fig. 8). The 1-mode model gives a good approximation of the experimental data, but the 3-mode model is in an even better agreement. This remains true for times as long as $\tau \approx 10$.

The previous comparisons were for high Atwood number. For low Atwood number, *At = 0.2*, a simulation has been carried out and harmonics growths have been compared with theory. This comparison is presented in Fig. 9. As before, the agreement is quite good and the negative value of the third harmonics is correctly predicted.

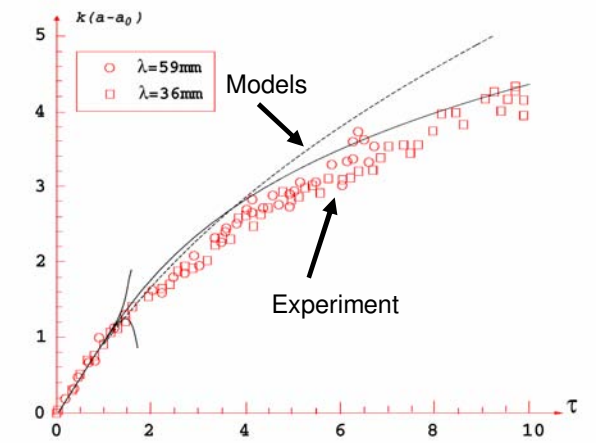

Fig. 8: *Half peak-to-valley amplitude for experimental data[4] (symbols), 1-mode model (dashed line) and 3-mode model (full line).*

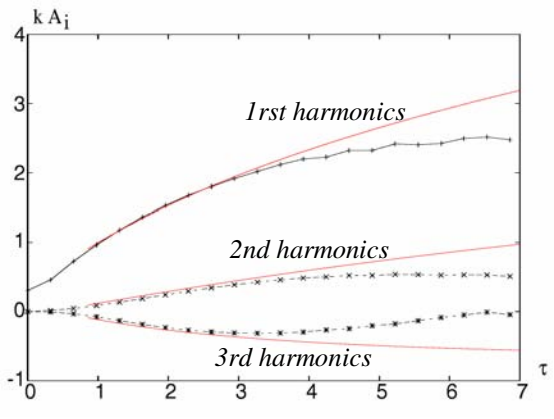

Fig. 9: *The same as in Fig. 7 but for At=0.2.*

Some models[7,8,9] give the evolution of the bubble velocity as a function of time. We present in Fig. 10, comparisons between the results of these models and the one obtained with the 3-mode nonlinear model. Once again, the agreement between the different theories is very good. It has been checked that this good agreement is also true for high Atwood numbers.

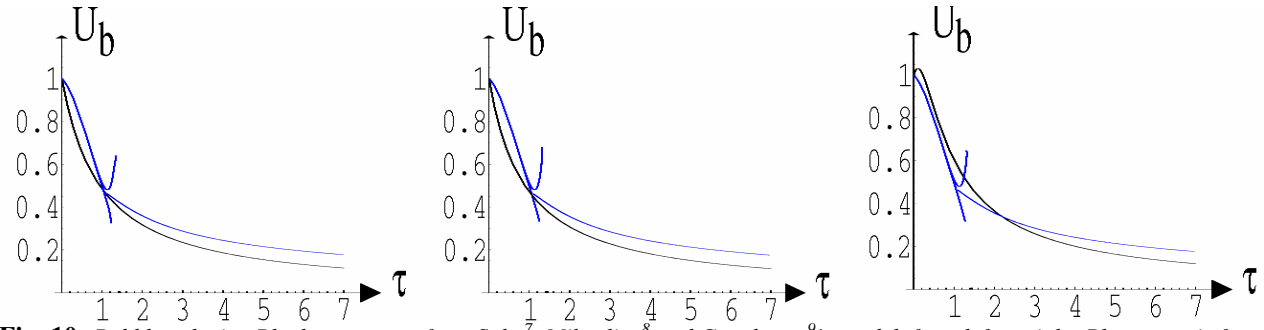

Fig. 10: *Bubble velocity. Black curves are from Sohn[7], Mikaelian[8] and Goncharov[9]'s model, from left to right. Blue curve is from the 3-mode nonlinear model with initial conditions by matching small perturbation method[1]. At=0.2.*

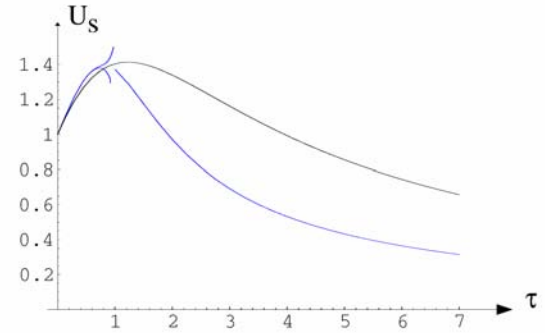

Fig. 11: *Spike velocity. . Black curve is from Sadot et al. model[10]. Blue curve is from the 3-mode nonlinear model with initial conditions by matching small perturbation method[1]. At=0.77.*

For the spike velocity, a comparison with Sadot *et al.* model[10] has been done for $At = 0.77$. The results are presented in Fig. 11. Some discrepancies can be observed between the two models.

As the 3-mode model give the growth of the first three harmonics, a shape of the interface can be built, even if it will remain single-evaluated. For the case $At = 0.635$, we have compared the shape of the interface obtained either from simulation or from the model. These comparisons are presented in Fig. 12, for the non-dimensional time $\tau = 0.8, 1.2, 1.8, 3.0$.

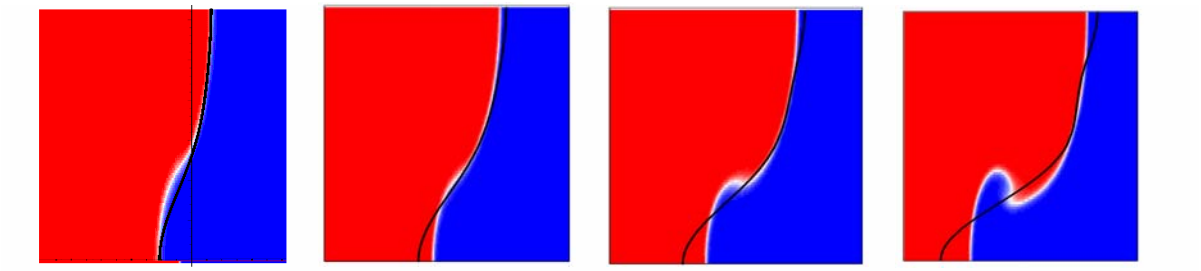

Fig. 12*: Shape of the interface. Comparison between model (blak line) and simulation (colored areas).* τ*=0.8, 1.2, 1.8, 3.0.*

As it can be seen, the shape of the bubble is very well estimated, even when the mushroom structure appears. On the other hand, the height of the spike is over-estimated in comparison with the simulation.

4. Concluding remarks and discussion

A new nonlinear model has been derived; it gives the growth of a single-mode perturbation for the IRM. The results are obtained by solving a set of coupled ordinary differential equations. Even if a complete mathematical demonstration is still in progress, the pseudo-solution which is obtained seems to be a good approximation of the exact solution. Indeed, several comparisons with both experimental, theoretical and numerical results show good agreements for a wide range of Atwood number. This remains true from linear to nonlinear regime.
Even if this nonlinear model cannot describe mushroom structures at the interface, this seems to have little effect on the peak-to-valley amplitude of the perturbation. However, at late time, the saturation of each harmonics seems under-estimated when compared with simulations. This underlines the need for a different mathematical formalism which could be able to describe mushroom structures.

But the simple formula: $\dot{A}_1(t) = k\,\mathrm{B}_1(0) \Big/ \sqrt{1+1/4k^2 A_1^2(t)}$, seems to give a simple means to roughly estimate the growth of a perturbation in the case of the Richtmyer-Meshkov instability. The 3-mode model, with the right initial conditions, seems to give even better results.

References

[1] M. Vandenboomgaerde, S. Gauthier and C. Mügler, Phys. Fluids **14**, 1111 (2002)
[2] Q. Zhang and S-I. Sohn, Phys. Fluids **9**, 1106 (1996).
[3] A.L. Velikovich and G. Dimonte, Phys. Rev. **76**, 3112 (1996).
[4] J.W. Jacobs and V.V. Krivets, « Experiments on the late-time development of single-mode Richtmyer-Meshkov instability ». Submitted to Physics of Fluids.
[5] J. Griffon and M. Boulet (CEA-DAM-Ile de France-Bruyères-Le-Châtel- France). Private communication.
[6] M. Olazabal (UMR-CELIA- Université Bordeaux I -France). Private communication.
[7] K.O. Mikaelian, Phys. Rev. E **67**, 026319 (2003)
[8] S-I. Sohn, Phys. Rev. E **67**, 026301 (2003)
[9] V.N. Goncharov, Phys. Rev. Lett. **88**, 134502 (2002)
[10] O. Sadot *et al.,* Phys. Rev. Lett. **80**, 1654 (1998)

Acknowledgements

We are grateful to :
J. Griffon and M. Boulet (CEA-DAM-Ile de France-Bruyères-Le-Châtel-France) for direct numerical simulations with TRICLADE code and discussions, and M. Olazabal (UMR-CELIA-Université Bordeaux I-France) for compressible linear perturbation computations with PERLE code.